Eurographics Conference on Visualization (EuroVis) 2026
N. Andrienko, M. Chen, and B. Wang
(Guest Editors)

COMPUTER GRAPHICS *forum*
Volume 45 (2026), Number 3

Uncertainty-Aware Visual Analysis of Force Networks in 2D Granular Materials

M. Evers[1,2], A. Naseer[3], T. G. Murthy[3], V. Natarajan[3], T. Bin Masood[4], D. Weiskopf[2] and I. Hotz[4]

[1]University of Siegen, Germany [2]University of Stuttgart, Germany [3]Indian Institute of Science, India [4]Linköping University, Sweden

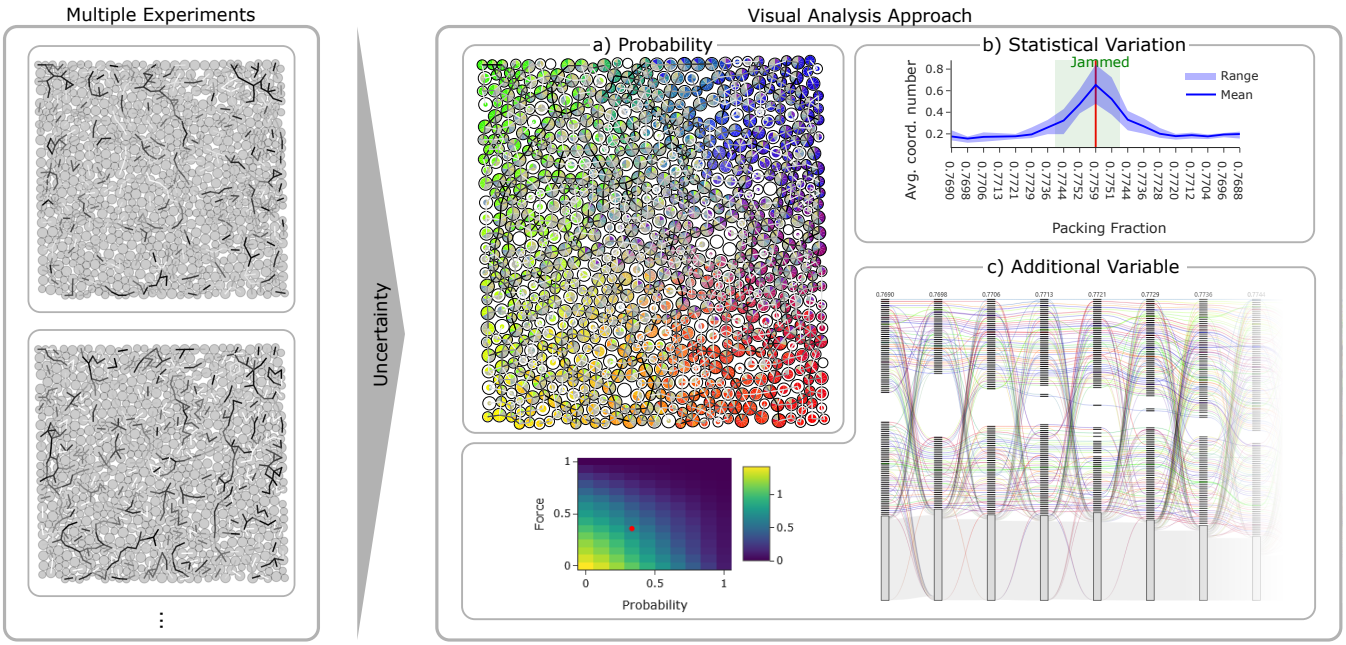

Figure 1: *Our approach combines different perspectives on uncertainty, which correspond to mental and mathematical models, for multiple experiments on granular material: a) The spatial view encodes the probability of occurrence of a spatial pattern such as a force chain. b) The variation of network descriptors such as the node degree over the packing fraction shows the uncertainty as variance. c) The heatmap treats the edge probability as a variable and uses it, similar to the force, to threshold edges while computing the Sankey diagram.*

Abstract

Uncertainty in experimental measurements makes it challenging to determine which features are intrinsic to the phenomenon and which are most stable and reliable. Granular materials, such as sand, form a complex system in which the forces between individual particles influence the material's macroscopic behavior. However, these forces are also subject to uncertainty, as repeated measurements can yield different results. In this paper, we investigate how to model and visually analyze the uncertain structure of forces in granular materials. We adopt different perspectives on uncertainty by considering it as variance, probability, or additional variable. For a nuanced analysis of granular material data, we propose combining visualizations that represent these perspectives into a single visual analytics approach. We integrate uncertainty-aware spatial visualizations that convey the probability of features, visualizations of derived measures and their variance over changes in the packing fraction, and overviews of varying probability thresholds. Finally, we evaluate our proposed approach in a case study conducted together with geotechnical engineers for the example of a 2D ensemble of photoelastic disks.

CCS Concepts

• ***Human-centered computing*** → ***Visualization techniques; Visual analytics;***

1. Introduction

Granular materials, such as sand, are composed of solid, macroscopic particles that exhibit complex force patterns between the particles [PMWT05, ZNL*17]. Understanding the formation of these force patterns is challenging because minor deviations in the system's parameters, such as the initial positions of the grains, can lead to changes in the individual forces between the particles and the formation of patterns on different scales. Therefore, even in highly controlled experiments, repeated measurements may yield different results. Thus, experiments can be conducted repeatedly to quantify the uncertainty and identify the most likely force patterns.

In this paper, we propose an uncertainty-aware analysis in so-called *force networks*, which are formed by treating the individual grains as nodes and the forces between them as weighted edges. As we consider highly controlled experiments where the initial particle positions are very similar, the main uncertainty in the system arises from the existence and force weighting of the edges. However, domain experts are not primarily interested in individual edges, but instead in mesoscopic (middle-scale) features, such as force chains, which correspond to connected components of the force network, and macroscopic features. While previous visualization approaches for granular material focus on feature extraction [RMM*23], tracking [RNN*24], and multi-scale analysis [RNM*26], they do not consider the data uncertainty. Visualization of an uncertain graph, independent of the application domain, traditionally aims at showing uncertainty in edges or nodes [vBW17b, CGH*24, GHL15, vKS*11, ZAH22, SNG*17]. In this paper, we instead focus on encoding the uncertainty of derived features. For a multifaceted analysis of the uncertain dataset, we combine visualizations at different aggregation levels, ranging from spatial details to an overview of the entire experiment, that also represent different mental (how the uncertainty is understood and used) and mathematical models of the underlying uncertainty (see Figure 1).

Based on this application scenario, we identify different perspectives to view the uncertainty. At first, the uncertainty describes a variance in macroscopic parameters, such as the number of particles without any forces to or from other particles. Second, the different realizations of the experiment are used to compute a probability of an observation, for example, the probability that a particle is part of a force chain. Third, the probability that a force exists between two particles can be treated as a variable and used for thresholding, allowing the user to interactively select the desired certainty required in the analysis.

In this paper, we first introduce the data in more detail (see Section 3) and discuss these different ways of treating uncertainty, which we derived from the application scenario (see Section 4). In Section 5, we describe how the different perspectives are incorporated in each visualization and how they are integrated in a visual analytics approach. We combine aggregated overview visualizations that show the evolution of the system if it is compressed and decompressed under external pressure with a glyph-based view that shows the spatial context for a fixed pressure. A Sankey diagram encodes changes of particles between connected components for user-defined force and uncertainty thresholds. Our approach was evaluated through case studies and interviews with domain experts, demonstrating the utility of combining different perspectives. In summary, our contributions are as follows.

- A discussion of different perspectives on uncertainty and how to combine them in a visual analytics system.
- A visualization of uncertain connected components that covers the uncertainty without requiring a dedicated matching.
- A visual analysis approach and workflow for analyzing uncertain structures in granular materials.
- A case study with domain experts to evaluate the usefulness of our approach that combines different views on uncertainty.

2. Related Work

In the following, we discuss related work to our approach. At first, we discuss visualization approaches that also target applications to granular materials followed by a discussion on uncertainty visualization beyond the domain of granular materials. Finally, we discuss existing usages of glyphs, which we will use to encode uncertainty in our spatial view.

Granular Materials. For a general overview of the use of visual computing for material science, we refer to Heinzl and Stappen [HS17]. While related applications such as the visualization of porous media [GVTA10, SKR*24] also make use of graph descriptions, they focus on connectivity structures or fluid flow through the material. ASEVis proposes an interactive approach to identifying user-defined features in active materials [EWL22], but its focus is on understanding dynamics and finding aggregations, rather than considering the uncertainty in the graph structure of the force network. Meier et al. [MSW*08] investigate multi-scale visualizations to connect micro- and macroscale information. While they also address the force network, they visualize only single measurements without considering uncertainty. Rasheed et al. [RMM*23, RNN*24, RNM*26] work on the same dataset as we do, but focus on extracting [RMM*23] and tracking [RNN*24] cycles that enclose particles without forces to and from other particles. To track the evolution over the experiment, they use a Sankey diagram, which we adopt in our paper and apply to the evolution of force chains. VisPhoD [RNM*26] provides a comprehensive analysis framework to analyze granular materials, but it does not focus on force chains or consider uncertainty explicitly.

Uncertainty Models. Uncertainty visualization is considered a challenging problem [KDJ*21]. A broad overview of different aspects of uncertainty visualization and its application in various domains can be found in a set of survey articles [HSB*22, Wei22, BHJ*14, PRJ11]. An attempt to characterize uncertainty has been made by Skeels et al. [SLSR08]. They discuss formats for uncertainty, including probabilities and ranges for quantified uncertainty, which closely relate to our perspectives on uncertain data. Peña-Araya et al. [PAFW*25] discuss the fuzziness of uncertainty based on a case study on geology. They find that many factors influence uncertainty and that it might vary during the analysis process. Gillmann et al. [GMR*23] discuss uncertainty in visual analytics. While they also discuss descriptions that relate to our perspectives, they mainly focus on sources of uncertainty in the visual analytics pipeline, which has been generalized to include uncertainty by Maack et al. [MSH*23]. Different sources of uncertainty are also

commonly discussed in other taxonomies for different application fields [Fis99, RPHL14, PPK*21]. We, however, focus on how to view uncertainty during the analysis process, where the uncertainty may be attributed to a single source.

Uncertainty in Graphs. On a more abstract data level, we consider graphs with uncertain edge weights. Existing approaches often focus on data mining in uncertain graphs, where an uncertain graph denotes a graph where each edge is associated with the probability that the corresponding nodes are connected [Ban22, KGPT17]. Common tasks include pattern extraction [JLA11, CZL*19], clustering [CFP*17, HGX*19, YWL*22], and graph decompositions [BGKV14]. Reachability queries, which are required to extract connected components, are known to be #P-complete, which means that they are at least NP-hard [JLDW11]. Thus, they are commonly computed based on samples, which are also referred to as possible worlds [PGPB14]. In this paper, we follow a similar approach by treating the measurements as samples of an unknown distribution. However, note that we differentiate not only whether an edge exists but also that existing edges are weighted. Visualization approaches for uncertain graphs often include the graph layout, for example, by combining splatting, edge bundling, and blending [SNG*17] or using animations of different possible outcomes [ZAH22]. In our case, each node corresponds to a particle with a physical location, and thus the node layout is already defined by the dataset. An alternative for encoding edge weight uncertainty uses visual variables on the edges [vBW17b, CGH*24, GHL15, vKS*11, SSSE16], as we also do for one of our spatial visualization options. However, these visualizations from prior work do not explicitly encode information on derived graph properties such as connected components.

Glyph-based Visualizations. Glyph-based visualizations are commonly used to visualize complex information [BKC*13, ROP11]. For example, glyphs can encode uncertainty in scalar fields [RGH*19], but without visualizing discrete features such as connected components. Cowe et al. [CNW*26] used pie-chart-based glyphs for multi-scale visualization but did not encode uncertainty. In this work, we use radial glyphs to visualize uncertain connected components [ERM*25], a visualization that Vehlow et al. [VBW17a] also used to indicate overlap in fuzzy communities.

3. Application Background, Data, and Tasks

This section summarizes information on the application domain, particularly the relation to data and task abstraction.

3.1. Data Acquisition and Description

In this paper, we focus on a 2D granular ensemble comprising photoelastic disks [DNM26]; the birefringent property of the disks is employed to quantify the contact forces between the disks. For detailed descriptions of the experimental setup, we refer to previous works [NDM26, RNN*24, RNM*26].

After preprocessing performed by the domain experts, one obtains a force network from the imaging data. This force network can be described as an undirected, weighted graph $G(V,E)$ where the nodes V are given as the disks. Each node $v \in V$ has a spatial location defined by the position of the corresponding disk and also associated with the radius of the disk. There is an edge $e \in E$ between two neighboring disks, which is weighted by the force that the two disks exert on each other. If there is no force, the weight $w(e) = 0$. As the nodes correspond to a 2D system, the resulting force network forms an embedded, planar graph.

During the course of the experiment, pressure is exerted on the set of disks. In the first stage, the loading stage, an increasing external pressure is exerted on the system, and in the unloading stage, the pressure is decreased. For higher pressures, the disks are more tightly packed, which can be quantified by the *packing fraction* of the disks, that is, the proportion of the total area occupied by the disks in the granular system. One goal of the experiment is to investigate the system's behavior over different packing fractions to understand the phenomenon of *jamming*, a macro property of the granular system, and its link to meso- and microscale properties of the system. Jamming occurs at higher packing fractions and is associated with phase transitions of the granular material.

The dataset we consider in this paper consists of 10 measurements with identical initial conditions. Each measurement consists of 8 to 17 steps with different packing fractions. Although the 10 measurements are repetitions of the same experimental setup, they deviate from each other. As the disks are manually placed according to their initial conditions, there might be small deviations in their positions. Due to the complexity and nonlinearity of the underlying system, these small deviations might amplify when exerting pressure and lead to larger differences in the resulting force networks. In the following, individual measurements are referred to as *realization* of the possible experimental behavior.

Thus, measurements can be seen as samples of a probability distribution that models the uncertainty of the system's behavior. We considered modeling the distributions explicitly. However, with only 10 measurements corresponding to 10 samples, a statistically meaningful modeling is not possible and could easily lead to overfitting. As performing the experiment is very time-consuming, obtaining more measurements is not feasible. Therefore, we instead decided to work on the sample level and use the 10 measurements as samples of the underlying distribution.

3.2. Analysis Tasks

In contrast to previous work [RNM*26], we focus on a joint analysis of all measurements as a single uncertain dataset instead of comparing individual measurements separately. Based on a discussion with the domain experts, who created the data, we identified a set of relevant analysis tasks in which the uncertainty should be taken into account and which we use to guide our visual design presented in Section 5:

T1: Identifying reliable structures. The measurement is repeated 10 times with approximately identical initial conditions to identify structures in the experiment that occur regularly. Thus, the goal is to find information with a high probability of occurring in a measurement. Structures that only rarely occur should be visualized while also communicating the uncertainty, such that the probability is conveyed to the analyst.

T2: Visualizing different scales. The main goal of the experiment is

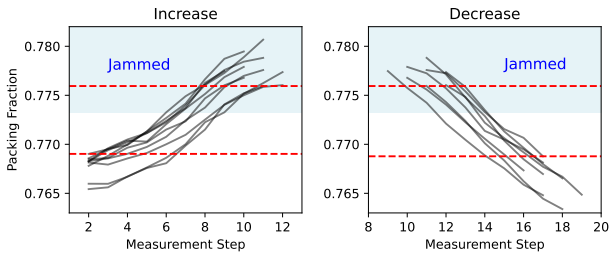

Figure 2: *For synchronizing the data between the different measurements (gray lines), only packing fractions between the two red dashed lines, which indicate the area where data for all ten (increase) or eight (decrease) measurements are available, are considered.*

to obtain an understanding of how structures on the microscale, such as forces between particles, relate to information on the macroscale, such as the number of nonparticipating nodes in the force network. Visualizations of both scales should include the uncertainty to avoid misinterpretations.

T3: Investigate the behavior when applying pressure. With increasing pressure, the packing fraction of the system increases. To better understand phase transitions in granular materials, the behavior of the system and associated uncertainty should be visualized as the packing fraction changes.

3.3. Data Alignment

The force networks in the raw data are not aligned, and there is no explicit correspondence between disks across realizations. For clarity, we will, in the following, refer to a set of realizations with a single packing fraction as a single step in the experiment. To treat data as realizations of the same underlying behavior, we need to perform an alignment.

First, we create a mapping between the individual disks based on their distances (see supplemental material for details). Next, we also needed to align the individual measurements based on the packing fraction of the different measurement steps. The packing fractions for individual measurements are shown in Figure 2. For consistency and completeness, we focus on the packing fraction range present in all measurements. Note that two experiments stop at the maximum increase of the packing fraction and do not contain a decrease. To still optimize the amount of data available but also consider that the decrease might lead to different effects, we treat the increase and the decrease in packing fraction differently. After obtaining the possible data range, we divide it into 19 equidistant steps such that the number of steps is symmetric around the maximum packing fraction and lies in the same range as the original number of steps. For the increasing steps, including the maximum, we take the joint range of all 10 measurements, while for the 9 decreasing steps, only 8 measurements are considered. For computing each realization, we use linear interpolation of adjacent measurements which can be considered a suitable approximation due to relatively small differences between adjacent steps. While the interpolation might introduce additional uncertainty, this uncertainty is small compared to the data uncertainty and is, thus, not explicitly considered in this paper.

4. Perspectives on Uncertainty

While existing work considers different formats [SLSR08] or descriptions [GMR*23] of uncertainty, its main focus is on combining uncertainty from different sources. Instead, we focus on combining multiple descriptions and usages of an uncertainty model to provide a more comprehensive view of the data, but we do not differentiate sources of uncertainty.

The uncertain data considered in this paper contains a set of measurements that can be used to quantify the system's uncertainty. However, the number of measurements is typically small because conducting the measurements is time-consuming. Therefore, we avoid estimating the underlying distribution directly and instead treat realizations as samples, thereby obtaining an implicit representation of the (unknown) probability distribution. Thus, the weight of each edge e can be described by a random variable $W(e)$ with probability distribution $p_{W(e)}(f)$ where f denotes the force. Note that the random variables of different edges are not independent. Since all explicit computations are based on samples, the dependencies between the different edges are also taken into account.

In the following, we will discuss different perspectives on how to work with this uncertainty model. The perspectives have been developed based on joint meetings and discussions with domain experts to understand their views on the data and to define analysis goals but are also grounded in the authors' previous experience with uncertainty modeling and visualization.

4.1. Uncertainty as Statistical Variation

One common description of uncertainty targets statistical variation. Especially for quantitative data, the uncertain value is associated with a variance or standard deviation. In this paper, we mainly use this description of uncertainty for macroscopic measures, which is a common approach from the domain expert's familiar analysis workflow. We include three different graph-based descriptors. To obtain a distribution over all measurements, the descriptors are first computed separately for each realization. The individual results can then be used to estimate the statistical variation over the entire experiment.

Node degree. The node degree is commonly analyzed as the so-called coordination number in the analysis of force networks to understand how densely connected the material is. Here, we consider the average node degree over the entire network, which corresponds to the average number of other disks that a disk interacts with. Thus, we compute for each experiment i the average node degree $\bar{k}_i = 2|E_i|/|V|$. We say that an edge exists if the weight $w(e) > F_t$, where F_t is a user-defined force threshold that can be changed interactively.

Connected component size. The average size of the connected components indicates whether large or small structures form in the granular material. Connected components are computed considering the edges with $w(e) > F_t$. To compute their size, the number of particles in each connected component is counted. According to the usual definition of connected components, a single node forms a

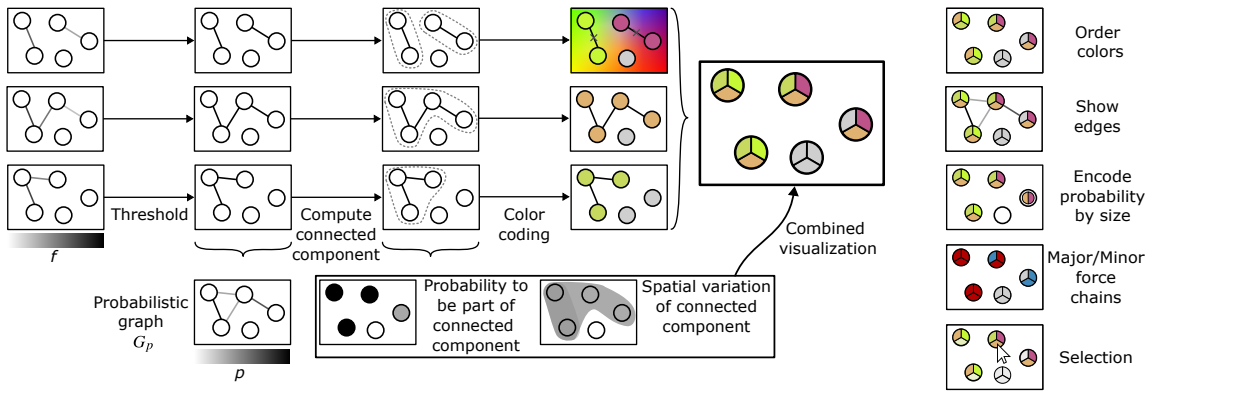

Figure 3: *The figure shows schematically how the spatial view is created (top-left), the different derived information that is included (bottom-left), and which different visual encodings are supported (right). The different visual encodings can also be combined.*

connected component of size one. However, since the disks corresponding to these nodes do not form force chains, we consider only connected components that contain at least two distinct nodes.

Number of non-participating nodes. Disks that do not experience or exert forces on other nodes are also referred to as rattlers. These disks correspond to nodes $\{v \in V | \forall e \in E(v) : w(e) \leq F_t\}$ where $E(v)$ denotes the set of incident edges to v. Counting the number of these non-participating nodes gives an overview of how many nodes do not participate in the interactions of the system.

4.2. Uncertainty as Probability

An alternative view of the data's uncertainty is to express it as a probability. Probability as a measure for uncertainty is common in everyday life [VHW25]. In the context of our work, probability indicates the chance that a feature in the data exists.

On the microscopic level, the probability $w_p(e)$ for an edge $e = (v_1, v_2) \in E$ indicates how probable it is that there is a force $w(e)$ larger than a user-defined threshold F_t between the disks corresponding to nodes $v_1, v_2 \in V$. Starting from the probability distribution function $p_{W(e)}(f)$, the probability that an edge with a strong enough force exists can be computed as

$$w_p(e) = \int_{F_t}^{\infty} p_{W(e)}(f) \mathrm{d}f \, . \tag{1}$$

For the sampling-based computation in this work, we divide the number of realizations in which the force is exceeded by the total number of measurements. Thus, we obtain a probabilistic graph G_p where each edge is weighted by the probability $w_p(e)$.

Additionally, our goal is to obtain the probability that a node belongs to a connected component, indicating that it participates in force propagation. At the same time, the spatial positions of the connected components in the 2D embedded graph could be associated with uncertainty. Therefore, we want to include both aspects. The computation of the uncertain connected components is illustrated in Figure 3. First, we compute the connected components $c^{(m)}$ based on the force threshold F_t for each measurement m. The computations are directly applied to the individual measurement results, rather than using the probabilistic graph, due to computational complexity and to account for covariances not included in the edge probabilities. Combining the connected components computed across different measurements not only allows consideration of spatial variability (see Section 5.3 for details) but also enables identification of the probability

$$p_{CC}(v) = \frac{|\{m \in \{0, \ldots, M-1\} \, | \, |c^{(m)}(v)| > 1\}|}{M} \tag{2}$$

that a node v belongs to a connected component, where $c^{(m)}(v)$ denotes the connected component to which node v belongs in measurement m of M measurements in total.

4.3. Uncertainty as Additional Variable

Unlike the previous sections that focused on mathematical models or descriptions [GMR*23] of uncertainty, this section addresses how the uncertainty value can be used. Often, uncertainty is considered integrated with other values, for example, with the mean. In contrast, the quantified uncertainty can be seen as an additional variable. Besides mapping it to a visual channel, such as color, this also enables processing operations, such as using uncertainty for filtering. While these approaches could, in principle, be applied to different (scalar) quantifications of uncertainty, we focus on probability in this work.

Starting from the probabilistic graph G_p, a threshold P_t, which is defined interactively by the users, can be used for filtering the edges such that only edges with $w_p(e) > P_t$ are considered. This filtered graph is defined as $G_{p>P_t} = (V, E_{p>P_t})$ with $E_{p>P_t} = \{e \in E | w_p(e) > P_t\}$ Note that we also consider the probability threshold P_t for computing the measures by neglecting edges with $w_p(e) \leq P_t$. To support users in selecting meaningful thresholds, the macroscopic measures introduced in Section 4.1 can be visualized as a function of the two thresholds (see Section 5.2 for details on the visual encoding). In this work, we use the graph $G_{p>P_t}$ to encode the evolution of the system over changes in the packing fraction which we will visually encode using a Sankey diagram (see Section 5.4). Thus, no explicit encoding of uncertainty is inherent in this graph. Instead, it is encoded implicitly by the user-defined threshold.

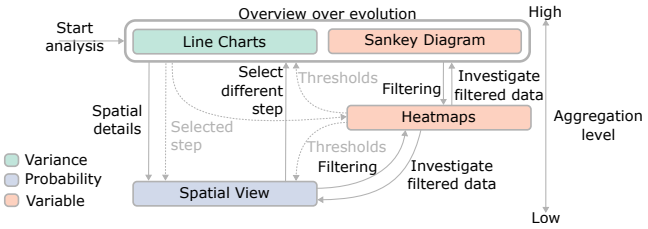

Figure 4: *The schematic diagram shows the user's workflow (solid arrows) and the impact of the selections (dashed arrows).*

5. Visual Analysis Process

In the following, we will first discuss our visual analytics approach and the workflow for analyzing granular material experiments with respect to the tasks presented above. The workflow was designed based on experience working on the same dataset, but with a focus on single experiments [RMM*23, RNN*24], and refined in joint meetings with the domain experts.

5.1. Overview and Workflow

Our visual analytics approach follows a navigation strategy that starts with an overview of the entire experiment, including all packing fractions, and proceeds to more detailed analyses based on user-defined filtering criteria [Shn96]. In contrast to alternative approaches [LBS*19], this mirrors the domain expert's common first step of identifying relevant packing fractions for further analysis. However, as explorative data analysis is an iterative process, the different levels of detail are closely linked (see Figure 4), thereby supporting analysis across different scales (task T2).

We adopt two approaches to show the system's evolution over the packing fraction (task T3): Line plots display changes in derived measures and their associated uncertainties. A Sankey diagram shows changes in the filtered graph $G_{p>P_t}$ and enables users to investigate connectivity changes across packing fractions (see Section 5.4 for details). When selecting a packing fraction in any visualization, all other visualizations are updated to either show the corresponding data or indicate the selected packing fraction. Heatmaps use color coding to indicate how the force threshold F_t and the probability threshold P_t affect the different measures, using the same measures as for the uncertain line plots. These plots provide additional information to inform threshold selection. A glyph visualization (see Section 5.3) conveys spatial information for the connected components, along with their uncertainty. The uncertainty encoding in the spatial view and the probability-based thresholding support the identification of reliable structures (task T1). The spatial information is also used to inform the color-coding in the Sankey diagram. Further, hovering over a box in the Sankey diagram highlights the corresponding spatial structure in the spatial view, facilitating bridging abstraction levels.

The visual analytics system is implemented as a web application using a Python backend with Plotly and Dash. The Sankey diagram and the spatial visualization are realized using D3 [BOH11]. The source code is available at `https://github.com/marinaevers/uncertain-force-networks`.

5.2. Measure Visualizations

We compute three graph-based measures, as discussed in Section 4.1, and visualize them using line charts and heatmaps. These measures are aggregated over the spatial domain and thus provide information at a larger scale, addressing part of task T2. To investigate behavior as a function of packing fraction (task T3), we chose to show a *line chart* (see Figure 1b) for each measure. As the underlying data uncertainty propagates to the final result, it can be visualized using color bands, which is a common approach that encodes uncertainty as variance. Due to the small number of realizations, we use the full range instead of smaller percentiles or the standard deviation. Based on discussions with domain experts, the visualization is enriched by domain-specific information. To facilitate analysis, the packing fraction range classified as jammed is highlighted with a green background color. A horizontal red line highlights the currently selected time step.

To support informed decisions for choosing the thresholds, the measures are shown as *heatmaps* for varying potential threshold values (see Figure 1c, left) using the uncertainty as a variable for thresholding (task T1). The visualizations are also used to interactively select the threshold by clicking within them. A red dot indicates the currently selected threshold. To avoid misinterpretation, we set the probability threshold resolution based on the number of distinct realizations for each packing fraction (in our case, 10 or 8), allowing us to derive this parameter directly from the dataset. Note that, due to the temporal demand for the experiment, the number of measurements is usually small. Otherwise, a fixed resolution could be used here. For the force threshold, we use a fixed resolution of 15, but the heatmap resolution can be easily adapted. Calculating the measures shown in the heatmap can take several seconds (see Section 6.1). Therefore, the heatmaps for each packing fraction are precomputed. To provide a direct visual link to the evolution, we show the heatmaps for the different measures directly next to the corresponding line charts.

5.3. Spatial Visualization

The spatial visualization supports visualization of the microscale (task T2) and should encode uncertainty to assess the reliability of the structure (task T1). We use a glyph-based visualization, building on radial glyphs [ERM*25, VBW17a], in which each glyph represents a disk (see Figure 1a,). The glyph is designed to show the probability of belonging to a connected component and the spatial variation among different connected components. We aim for a visual encoding in which small spatial variations appear less prominent than large variations. While matching components, for example, based on graph matching approaches, would support a direct quantification of this spatial variation, the desired outcome for larger variations is not always clear. Thus, finding a meaningful matching heuristic is challenging. Therefore, we use visual similarities rather than establishing explicit correspondences between the different measurements. Figure 3 shows an illustration of how this view is created.

An alternative to glyphs is to use edges rather than nodes. However, this results in more visual clutter, as even in planar graphs, the number of edges is often higher than the number of nodes. Each disk

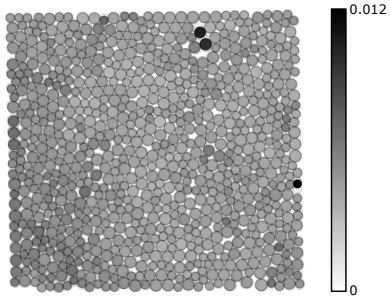

Figure 5: *The spatial variation of the disks is visualized by color-coding the standard deviations and showing the different positions with reduced opacity. For most disks, there is little variation.*

is encoded by a radial glyph whose size corresponds to the disk's size. For the glyph positions, we use the average positions over all measurements. Because position deviations are mostly very small and the original disks do not overlap, this prevents glyph overlap and defines the graph's spatial layout. Each slice of the radial glyph corresponds to one realization. We enhance the glyph-based visualization by showing the probabilistic graph G_p. The probabilities are encoded using a white-to-black colormap along the edges, so that the most probable edges are drawn in black and are thus clearly distinguishable from the glyphs.

Spatial variation. The colors of the slices are determined by the spatial positions of the connected components. For each connected component with at least two nodes, we compute the barycenter. Then, we use the spatial position of the barycenter to assign a color of a 2D colormap [SBT*15, RNN*24] to the corresponding component (see Figure 3). Similar colors across different slices indicate that the corresponding connected components have a large spatial overlap, while different colors indicate more spatial separation. Within the paper, we use the same 2D colormap that was used in previous work and is familiar to the domain experts [RNN*24], but the colormap could be exchanged easily.

For interpreting the force chains, it is important for domain experts to be able to map the information back to variations in disk positions. Therefore, users can activate a deviation view, which uses a white-to-black color scale to encode the standard deviation of the particle positions. For more detailed information on the spatial deviation, we render the outlines of the particles with reduced opacity, as shown in Figure 5.

Non-participating nodes. For individual nodes that do not interact with others, we use a light gray that is not part of the 2D color map. We choose a less prominent color to indicate that these nodes do not contribute to the force propagation. Thus, the percentage of colorful slices indicates the probability that a node belongs to a connected component. An alternative encoding uses the glyph's size to encode probability, so that larger glyphs have a higher probability than smaller ones. To maintain the disk size encoding, a black outline shows the disk's original size, and the relative sizes with respect to the outline encode the probability. Here, we use the circle's area as a visual channel. Even though recent work [KRF25] found that the use of area encodings over length encodings in circle sectors in closely related rose charts depends on the encoded size, we see the strength of the size encoding in our case to quickly identify very high or very low probabilities. For estimating exact percentages, we expect the alternative encoding using light gray slices to perform better. To leverage the advantages of both encodings, the user can interactively switch. A comparison of the different options is shown in Figure 3 (right).

Major and minor force chains. Based on the domain experts' feedback, we also support the explicit domain-specific encoding of so-called major and minor force chains in the visualization which helps to identify reliable structure (task T1). They differentiate between these two types of force chains based on an additional force threshold: major force chains are linked to forces above the threshold, and minor force chains are linked to forces below it. By default, they use the average across all forces as a threshold, which we also use in this paper. Alternatively, users can use the threshold F_t to separate major and minor force chains. Major force chains are encoded in red, while minor ones are shown in blue. Using only two colors allows differentiation between the two features but no longer shows the spatial variations of individual components. An example for this encoding is shown in Figure 3.

Slice ordering. By default, we order the slices in the glyphs according to the initial order of the measurements, starting from the top middle and proceeding clockwise. Keeping the same order for all individual glyphs allows for seeing relations such as correlations between the disks. However, this makes it hard to estimate the probability of belonging to the same component. Therefore, we allow users to activate reordering based on color similarity, so that similar colors, which should correspond to similar spatial positions of the components, are grouped close together. To compute the color order, we start with the first component and find the component with the closest barycenter, which is shown second. Then, we proceed iteratively. The light gray slices are always grouped together and shown last. When clicking on a disk, all slices belonging to other components are desaturated (see Figure 3, bottom right).

One important aspect when creating the spatial view is to ensure convergence as the number of measurements increases, to be consistent with the view that the realizations are samples from an unknown underlying distribution. One common analysis step does further aggregations over different packing fractions. Given that the jammed phase is especially relevant, aggregating the dataset analyzed in this paper would yield 38 individual realizations, which should be displayed simultaneously. Especially with the predefined ordering, our visualizations support showing many realizations at once. While the main focus of our work is analyzing the entire experiment to represent an uncertain system, it is also possible to select a single measurement, which is then shown individually.

5.4. Sankey Diagram

Finally, the variations of the force chains should be visualized over the changes in the packing fraction to identify their reaction to the external pressure (task T3). This evolution is visualized using a Sankey diagram, which shows the sizes of the connected components but also split and merge events (see Figure 6b). Each node in the Sankey diagram corresponds to a connected component, and

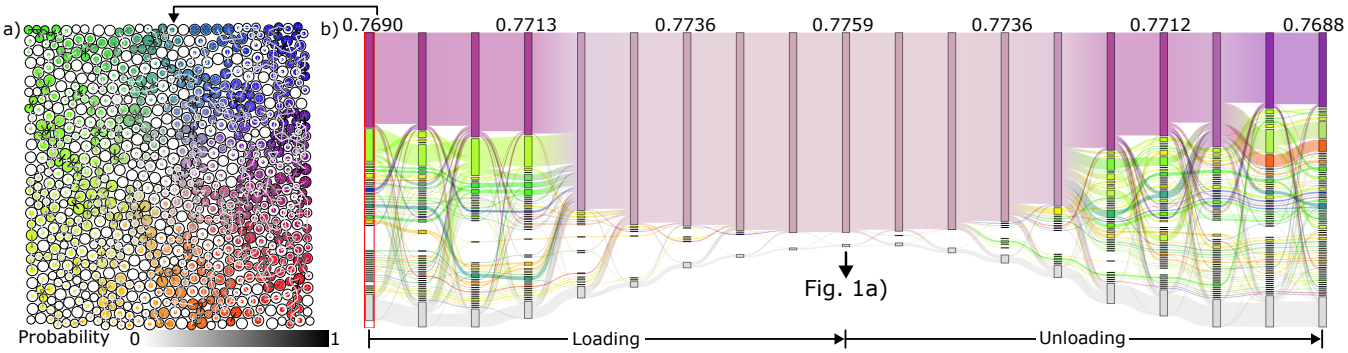

Figure 6: *The Sankey diagram (b) is computed based on connected components in the probabilistic graph G_p, which is shown as color-coded edges in the spatial views for the first step (a).*

transitions indicate how the connected components change as the system load varies. Node size represents the size of the connected components, and color encodes the position in the spatial domain. Here, we apply the same color coding based on barycenters as for the spatial view. The non-participating nodes are aggregated into one node shown in light gray. While the Sankey diagram was used in previous work [RNN*24] to show the evolution of cycles in this data, we instead show the connected components of the graph $G_{p>P_t}$. By investigating connected components of $G_{p>P_t}$, the general force structure is evaluated, while the uncertainty is indirectly encoded as a variable for thresholding the probability.

The Sankey diagram can be used to select an individual packing fraction for a more detailed analysis in other views. The currently selected packing fraction is highlighted with a red box. It is also possible to select a node in the Sankey diagram. To provide more spatial context, the corresponding disks are highlighted in the spatial view by thickening their outline. Therefore, the spatial information remains visible.

6. Evaluation

In the following, we first discuss algorithmic evaluations of computation time and scalability for key components of the visual analytics system based on synthetic data. After that, we discuss a case study and feedback from domain and visualization experts.

6.1. Convergence and Computation Times

To validate that our sampling strategy and our visual similarity approximate the ground truth, we validate the convergence. For comparison against the ground truth, we use a small synthetic dataset (see Figure 7) defined by using Gaussian distributions for the force distributions of the edges, where the edges are independent of each other. This allows us to compute the ground truth for the connected components, shown in Figure 7. The ground truth is computed by considering all possible connected components and determining their probability by multiplying the edge probabilities. By visually investigating the results for different sample sizes, we see that the visualization approximates the one of the ground truth and, thus, shows the desired behavior. To quantify computation times and

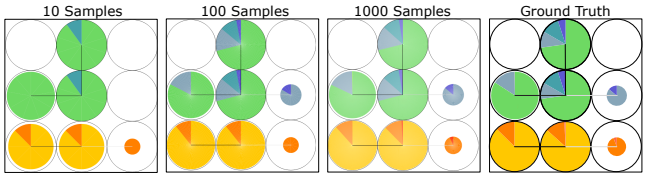

Figure 7: *When increasing the number of samples created from a synthetic dataset, our sample-based computation converges toward the analytically computed ground truth.*

investigate scalability with respect to problem size, we upscale the synthetic dataset by varying the number of disks, the number of measurements per packing fraction, and the number of packing fraction steps. All timings were recorded using an AMD Ryzen 9 9900X 12-core processor (detailed evaluations are provided in the supplemental material). For the real dataset, all computations are performed within a few seconds (see the video for the interaction).

6.2. Case Study

We evaluate our approach on real-world data with two domain experts (5 years and 16 years of experience in the domain of granular materials), both of whom are authors of this paper. In a first formative assessment, we aimed to gain a deeper understanding of the insights they want from data analysis and their current analysis workflow, and to receive feedback on an initial prototype. We used their feedback to improve our visual analytics solution. We conducted a summative assessment spread over several meetings with the same domain experts who had also participated in the initial meeting. In between, we provided our visual analytics solution via web-based hosting, which allowed domain scientists to use the tool and explore their data independently [SMM12]. Finally, one of the domain experts completed an online questionnaire comprising raw NASA-TLX and four questions to rate the intuitiveness of the different views of uncertainty and their interpretations on a 7-point Likert scale. More details on the structure of the meetings and the questionnaires used to prompt the semistructured interviews are available in the supplemental material. The following analysis, including more details, is also shown in the supplemental video.

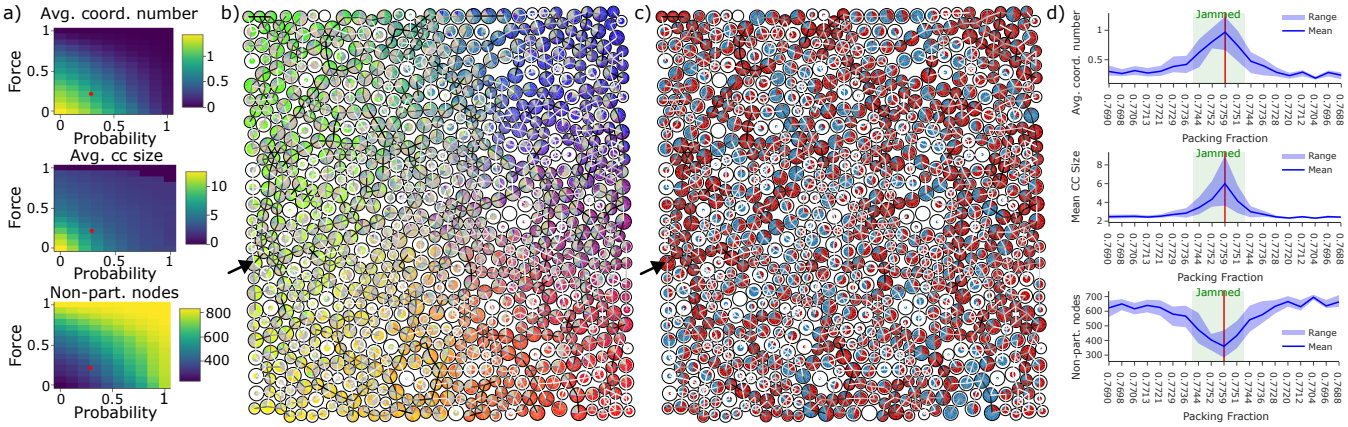

Figure 8: *Heatmaps (a) show the changes of the measure for different probability and force thresholds. When choosing a force threshold $F_t = 0.21$ and aggregating over all jammed states, the spatial view (b) shows several certain force chains. Using red for major force chains and blue for minor ones (c) provides information on the strength of the force chains. The arrow points to a large, chain-like structure that appears in all experiments. The line charts (d) show the evolution of the measures and their uncertainty over the course of the experiment for an additional probability threshold $P_t = 28\%$.*

To obtain an overview of the evolution of the experiment (task T3), the Sankey diagram can be investigated (see Figure 6b). Considering all forces, several small, connected components are visible, along with one larger component for the unjammed state. In the jammed state, there are forces between most of the disks, consistent with expectations for jammed materials. The evolution overview of the different measures shows the expected behavior with a maximum in the expected value of average coordination number and average connected component size, as well as the minimum expected number of non-participating nodes for the highest packing fraction. However, the variation in general is very large, especially for the average connected component size. This hints toward large variations in the connected components, which would agree with surprisingly strong differences that were found in previous work [RNM*26] and might be linked to instabilities studied in percolation theory [LLL*21].

To confirm the hypothesis, the spatial view can be used (see Figure 1a). A large amount of color variation inside the glyphs confirms the large differences in the spatial extent of the individual force chains and, thus, explains the high uncertainty of the data and allows for a connection between observations on the small and local scale to the high variance on more global observations (task T2). At the same time, a high number of fully filled glyphs shows a high agreement of the corresponding disks contributing to the force propagation. Showing the edges with the probability encoding, together with the general probability of the disks, reveals chain-like structures, for example, in the left part of the material.

To focus on stronger forces, the force threshold F_t can be increased. The heatmap reveals that the expected average connected component size decreases quickly with higher force thresholds, while the other two measures exhibit slower changes (see Figure 8a). Based on the heatmaps, the threshold is set to $F_t = 0.21$, for which several chain-like structures remain visible in the spatial view (see Figure 8b). To investigate the force chains in the jammed states, all jammed realizations are aggregated in this figure. Investigating major and minor force chains (see Figure 8c) shows that several connected components persist over the entire jammed region and also contribute to force chains with high forces because the majority of the glyphs is red. To further emphasize reliable structures (task T1), the force threshold can be increased such that only edges with a probability of more than 28% are considered. This slightly decreases the variance across the different measures as shown in Figure 8d. When investigating the Sankey diagram with the new thresholds, the step with the highest packing fraction remains dominated by one large component (see supplemental material, Figure 4). While there is no perfect symmetry in the loading (increase of packing fraction) and unloading phase (decrease of packing fraction), some structures appear very similar, both in the loading and unloading phase (see supplemental material, Figure 4), while others, such as the green component (see green arrows), split up into several components.

6.3. Domain Expert Feedback

Overall, the domain experts' feedback on the visual analysis approach was very positive, and they stated that it is a very helpful tool. The domain expert who explored the tool most rated the perspectives and their combination as intuitive (ratings 5-6 on a 7-point Likert scale where 7 is very intuitive). The joint look at the entire dataset fills a gap in their previous analysis workflow. One of the experts stated: "The reason we did this experiment, like this, not changing particle configuration in 10 different experiments, was that we wanted to see what the similarity is in the force network. [...] We couldn't find any descriptor which would tell us that there is some similarity." Thus, the analysis task of identifying reliable structures (task T1) could not be solved with their previous analysis methods, limiting also the inclusion of uncertainty in the other analysis tasks. However, we also observed a learning curve. After the first exploration phase, during which one of the experts spent time exploring the tool, several additional questions could be clarified in the subsequent meeting.

Relevance for domain. The domain experts expressed their interest in incorporating the work into their usual analysis workflow. They also proposed including it in a methods wiki for analyzing photoelasticity data (photoelasticity.net), as they see the utility for other researchers in their community. They also emphasize the importance of making the implemented software easy to use across different datasets, recognizing the approach's value not only for their own work in other projects but also for colleagues who perform photoelastic experiments. In the following, we will discuss the feedback on the different views and the underlying uncertainty perspectives in more detail.

Statistical variation. Looking at the variance of aggregated measures is a procedure that is also commonly done in existing workflows. In the initial meeting, they stated that examining statistical data is a common process when analyzing their experimental results. One of the experts said: "One thing about it is, yes, that can be done by me as well without using the visualization tool, but what is different here is, it is very interactive, just by changing the mouse marker and selecting the force and probability values," which indicates that they value the close linking between the different visualizations and the different perspectives on the data but are also very familiar with this percpective on uncertainty.

Probability. While this perspective was not used in their previous workflows, the concept was easily understood. One of the participants said: "I think that is very new because it instantaneously lets you know which particles are taking part in the force transmission and what is the probability of them taking part in the force transmission," which indicates that this view addresses a previously open problem. They rated the glyph visualization as "understandable to anyone in our field." The clear understanding and utility of the view for their analysis workflow also became visible when they asked about extending the additional aggregated view over different packing fractions.

Uncertainty as a variable. Several questions regarding the thresholding indicate a higher complexity compared to the other two concepts. However, they particularly valued the ability to interactively adjust thresholds and investigate their impact on statistical variation. Discussions for the use case, the use of heatmaps, and a score of 6 on a 7-point Likert scale for the intuitiveness indicate that the concept of using uncertainty as a variable was well understood. While both domain experts had worked with the Sankey diagram before [RNN*24], they still considered it a relatively complex visualization and asked for possibilities to simplify it. However, they stated that the interactive linking, especially to the spatial view, helps in understanding it. Therefore, the difficulties might arise from the higher abstraction level of the data compared to the other visualizations, rather than from the perspective on uncertainty.

6.4. Visualization Expert Study

We employ the ICE-T test [WAM*19] for a heuristic quantification of the value of our visualization [Sta14]. As an alternative to our glyph-based encoding, we replaced the spatial view with small multiples representing the individual realizations while maintaining the other views. All participants completed an online survey that began with an introduction to the approach and the application domain. Next, they explored the interactive visual analysis tool where the order of the two visual encodings was randomized, answered the ICE-T test questions with the option to add comments for each visual encoding, and completed demographic questions. We received 16 responses from visualization experts with 2 to 24 years of experience (mean: 8.7 years); two participants reported difficulty understanding the approach. We followed the guidelines by Wall et al. [WAM*19] for evaluating the results, including hierarchical averaging. Detailed figures are available in the supplemental material. Overall, we observed a strong variation between participants such that no approach clearly dominates. However, we obtained an overall score of 5.39 with a standard deviation of 0.56 for small multiples and 5.56 with a standard deviation of 0.61 for the glyph view, indicating that both representations are rated as valuable. Similar values were achieved for the individual dimensions insight, time, essence, and confidence (see supplemental material).

7. Conclusion and Future Work

We presented a visual analytics approach to investigate force networks and their uncertainty in granular materials. Based on several measurements, we quantify the uncertainty as both variances and probabilities, and also use it as a variable for thresholding, which allows filtering for more likely structures. Combining multiple visualizations allows for identifying force chains and their uncertainty (task T1), viewing the data at different scales (task T2), and investigating changes over the course of the experiment (task T3). Feedback from domain experts indicates their interest in applying the approach to other datasets and its general relevance to the domain. Based on the application example, we showed the usefulness of combining different perspectives on uncertain data into a joint analysis. Combining different views on uncertainty, including mental and mathematical models, is also applicable in other domains where a more nuanced and comprehensive view of the data is beneficial. Our evaluation shows that our approach visually scales well with increasing sample sizes and converges toward the ground truth of the underlying distributions. While our approach supports the number of disks as commonly used in photoelastic disk experiments, spatial aggregation could further improve the scalability.

Future work could include investigating uncertainty in other spatial structures in granular materials, such as cycles [RMM*23]. A generalization of the spatial visualization that does not rely on spatial alignment would allow a broader applicability not only to datasets studying granular materials without fixed initial conditions but also in other domains. While our domain expert interviews show the utility of the spatial visualization for the given use case, a task-based user study could provide more insights into the general applicability for visualizing uncertain connected components.

Acknowledgments

This work was supported by the Deutsche Forschungsgemeinschaft (DFG, German Research Foundation) – Project-ID 251654672 – TRR 161 and by the Swedish e-Science Research Center (SeRC), the ELLIIT environment for strategic research in Sweden, and the Swedish Research Council (VR) grants 2019-05487 and 2023-04806. We used Grammarly solely for grammar correction and language polishing.

References

[Ban22] BANERJEE S.: A survey on mining and analysis of uncertain graphs. *Knowledge and Information Systems 64*, 7 (2022), 1653–1689. doi:10.1007/s10115-022-01681-w. 3

[BGKV14] BONCHI F., GULLO F., KALTENBRUNNER A., VOLKOVICH Y.: Core decomposition of uncertain graphs. In *Proceedings of the 20th ACM SIGKDD International Conference on Knowledge Discovery and Data Mining* (2014), ACM, pp. 1316–1325. doi:10.1145/2623330.2623655. 3

[BHJ*14] BONNEAU G.-P., HEGE H.-C., JOHNSON C. R., OLIVEIRA M. M., POTTER K., RHEINGANS P., SCHULTZ T.: Overview and state-of-the-art of uncertainty visualization. In *Scientific Visualization*. Springer, 2014, pp. 3–27. doi:10.1007/978-1-4471-6497-5_1. 2

[BKC*13] BORGO R., KEHRER J., CHUNG D. H. S., MAGUIRE E., LARAMEE R. S., HAUSER H., WARD M., CHEN M.: Glyph-based visualization: Foundations, design guidelines, techniques and applications. In *Eurographics 2013 - State of the Art Reports* (2013), The Eurographics Association. doi:10.2312/conf/EG2013/stars/039-063. 3

[BOH11] BOSTOCK M., OGIEVETSKY V., HEER J.: D^3 Data-driven documents. *IEEE Transactions on Visualization and Computer Graphics 17*, 12 (2011), 2301–2309. doi:10.1109/TVCG.2011.185. 6

[CFP*17] CECCARELLO M., FANTOZZI C., PIETRACAPRINA A., PUCCI G., VANDIN F.: Clustering uncertain graphs. *Proceedings of the VLDB Endowment 11*, 4 (2017), 472–484. doi:10.1145/3186728.3164143. 3

[CGH*24] CONROY M., GILLMANN C., HARVEY F., MCHEDLIDZE T., FABRIKANT S. I., WINDHAGER F., SCHEUERMANN G., TANGHERLINI T. R., WARREN C. N., WEINGART S. B., REHBEIN M., BÖRNER K., ELO K., JÄNICKE S., KERREN A., NÖLLENBURG M., DWYER T., EIDE Ø., KOBOUROV S., BETZ G.: Uncertainty in humanities network visualization. *Frontiers in Communication 8* (2024). doi:10.3389/fcomm.2023.1305137. 2, 3

[CNW*26] COWE A., NEUROTH T., WU Q., RIETH M., CHEN J., LEE M., MA K.-L.: Glyph-based multi-scale visualization of spatial turbulent multi-physics statistics. *Computer Graphics Forum* (2026), e70399. In press. doi:10.1111/cgf.70399. 3

[CZL*19] CHEN Y., ZHAO X., LIN X., WANG Y., GUO D.: Efficient mining of frequent patterns on uncertain graphs. *IEEE Transactions on Knowledge and Data Engineering 31*, 2 (2019), 287–300. doi:10.1109/TKDE.2018.2830336. 3

[DNM26] DANIELS K. E., NASEER A., MURTHY T. G.: Data from: Micromechanics of compressive and tensile forces in partially-bonded granular materials [Dataset], 2026. doi:10.5061/dryad.9kd51c5z0. 3

[ERM*25] EVERS M., RASHEED F., MASOOD T. B., HOTZ I., WEISKOPF D.: Pie chart glyph visualization of uncertain connected components. In *EuroVis 2025 - Posters* (2025), The Eurographics Association. doi:10.2312/evp.20251131. 3, 6

[EWL22] EVERS M., WITTKOWSKI R., LINSEN L.: ASEVis: Visual exploration of active system ensembles to define characteristic measures. In *2022 IEEE Visualization and Visual Analytics* (2022), IEEE, pp. 150–154. doi:10.1109/VIS54862.2022.00039. 2

[Fis99] FISHER P. F.: Models of uncertainty in spatial data. In *Geographical Information Systems. Volume 1: Principles and Technical Issues*. John Wiley & Sons, 1999, pp. 191–205. 3

[GHL15] GUO H., HUANG J., LAIDLAW D. H.: Representing uncertainty in graph edges: An evaluation of paired visual variables. *IEEE Transactions on Visualization and Computer Graphics 21*, 10 (2015), 1173–1186. doi:10.1109/TVCG.2015.2424872. 2, 3

[GMR*23] GILLMANN C., MAACK R. G. C., RAITH F., PÉREZ J. F., SCHEUERMANN G.: A taxonomy of uncertainty events in visual analytics. *IEEE Computer Graphics and Applications 43*, 5 (2023), 62–71. doi:10.1109/MCG.2023.3299297. 2, 4, 5

[GVTA10] GRAU S., VERGÉS E., TOST D., AYALA D.: Exploration of porous structures with illustrative visualizations. *Computers & Graphics 34*, 4 (2010), 398–408. doi:10.1016/j.cag.2010.05.001. 2

[HGX*19] HAN K., GUI F., XIAO X., TANG J., HE Y., CAO Z., HUANG H.: Efficient and effective algorithms for clustering uncertain graphs. *Proceedings of the VLDB Endowment 12*, 6 (2019), 667–680. doi:10.14778/3311880.3311884. 3

[HS17] HEINZL C., STAPPEN S.: STAR: Visual computing in materials science. *Computer Graphics Forum 36*, 3 (2017), 647–666. doi:10.1111/cgf.13214. 2

[HSB*22] HÄGELE D., SCHULZ C., BESCHLE C., BOOTH H., BUTT M., BARTH A., DEUSSEN O., WEISKOPF D.: Uncertainty visualization: Fundamentals and recent developments. *it – Information Technology 64*, 4-5 (2022), 121–132. doi:10.1515/itit-2022-0033. 2

[JLA11] JIN R., LIU L., AGGARWAL C. C.: Discovering highly reliable subgraphs in uncertain graphs. In *Proceedings of the 17th ACM SIGKDD International Conference on Knowledge Discovery and Data Mining* (2011), ACM, pp. 992–1000. doi:10.1145/2020408.2020569. 3

[JLDW11] JIN R., LIU L., DING B., WANG H.: Distance-constraint reachability computation in uncertain graphs. *Proceedings of the VLDB Endowment 4*, 9 (2011), 551–562. doi:10.14778/2002938.2002941. 3

[KDJ*21] KAMAL A., DHAKAL P., JAVAID A. Y., DEVABHAKTUNI V. K., KAUR D., ZAIENTZ J., MARINIER R.: Recent advances and challenges in uncertainty visualization: a survey. *Journal of Visualization 24*, 5 (2021), 861–890. doi:10.1007/s12650-021-00755-1. 2

[KGPT17] KASSIANO V., GOUNARIS A., PAPADOPOULOS A. N., TSICHLAS K.: Mining uncertain graphs: An overview. In *International Workshop of Algorithmic Aspects of Cloud Computing* (2017), Springer, pp. 87–116. doi:10.1007/978-3-319-57045-7_6. 3

[KRF25] KIESEL D., RIEHMANN P., FROEHLICH B.: Rose charts: Area or length encoding for fill level of circle sectors? In *EuroVis 2025 - Short Papers* (2025), The Eurographics Association. doi:10.2312/evs.20251075. 7

[LBS*19] LUCIANI T., BURKS A., SUGIYAMA C., KOMPERDA J., MARAI G. E.: Details-first, show context, overview last: Supporting exploration of viscous fingers in large-scale ensemble simulations. *IEEE Transactions on Visualization and Computer Graphics 25*, 1 (2019), 1225–1235. doi:10.1109/TVCG.2018.2864849. 6

[LLL*21] LI M., LIU R.-R., LÜ L., HU M.-B., XU S., ZHANG Y.-C.: Percolation on complex networks: Theory and application. *Physics Reports 907* (2021), 1–68. doi:10.1016/j.physrep.2020.12.003. 9

[MSH*23] MAACK R. G., SCHEUERMANN G., HAGEN H., PEÑALOZA J. T. H., GILLMANN C.: Uncertainty-aware visual analytics: scope, opportunities, and challenges. *The Visual Computer 39*, 12 (2023), 6345–6366. doi:10.1007/s00371-022-02733-6. 2

[MSW*08] MEIER H. A., SCHLEMMER M., WAGNER C., KERREN A., HAGEN H., KUHL E., STEINMANN P.: Visualization of particle interactions in granular media. *IEEE Transactions on Visualization and Computer Graphics 14*, 5 (2008), 1110–1125. doi:10.1109/TVCG.2008.65. 2

[NDM26] NASEER A., DANIELS K. E., MURTHY T. G.: Micromechanics of compressive and tensile forces in partially bonded granular materials. *Physical Review Letters 136* (2026), 098201. doi:10.1103/9yny-wxfr. 3

[PAFW*25] PEÑA-ARAYA V., FONTAINE C. M., WEI X., DELPECH G., BEZERIANOS A.: Uncertainty in science is malleable. advocating for user-agency in defining uncertainty in visualizations: a case study in geology. In *Proceedings of the 2025 CHI Conference on Human Factors in Computing Systems* (2025), ACM. doi:10.1145/3706598.3713972. 2

[PGPB14] PARCHAS P., GULLO F., PAPADIAS D., BONCHI F.: The pursuit of a good possible world: Extracting representative instances of uncertain graphs. In *Proceedings of the 2014 ACM SIGMOD International*

Conference on Management of Data (2014), ACM, pp. 967–978. doi:10.1145/2588555.2593668. 3

[PMWT05] PETERS J., MUTHUSWAMY M., WIBOWO J., TORDESILLAS A.: Characterization of force chains in granular material. *Physical Review E—Statistical, Nonlinear, and Soft Matter Physics 72*, 4 (2005), 041307. doi:10.1103/PhysRevE.72.041307. 2

[PPK*21] PELZ P. F., PFETSCH M. E., KERSTING S., KOHLER M., MATEI A., MELZ T., PLATZ R., SCHAEFFNER M., ULBRICH S.: Types of uncertainty. In *Mastering Uncertainty in Mechanical Engineering*. Springer, 2021, pp. 25–42. doi:10.1007/978-3-030-78354-9_2. 3

[PRJ11] POTTER K., ROSEN P., JOHNSON C. R.: From quantification to visualization: A taxonomy of uncertainty visualization approaches. In *IFIP Working Conference on Uncertainty Quantification* (2011), Springer, pp. 226–249. doi:10.1007/978-3-642-32677-6_15. 2

[RGH*19] RISTOVSKI G., GARBERS N., HAHN H. K., PREUSSER T., LINSEN L.: Uncertainty-aware visual analysis of radiofrequency ablation simulations. *Computers & Graphics 79* (2019), 24–35. doi:10.1016/j.cag.2018.12.005. 3

[RMM*23] RASHEED F., MASOOD T. B., MURTHY T. G., NATARAJAN V., HOTZ I.: Multi-scale visual analysis of cycle characteristics in spatially-embedded graphs. *Visual Informatics 7*, 3 (2023), 49–58. doi:10.1016/j.visinf.2023.06.005. 2, 6, 10

[RNM*26] RASHEED F., NASEER A., MASOOD T. B., MURTHY T. G., NATARAJAN V., HOTZ I.: Explorative analysis of dynamic force networks in 2D photoelastic disks ensembles. *IEEE Transactions on Visualization and Computer Graphics 32*, 4 (2026), 3002–3015. doi:10.1109/TVCG.2026.3660683. 2, 3, 9

[RNN*24] RASHEED F., NASEER A., NILSSON E., MASOOD T. B., HOTZ I.: Multi-scale cycle tracking in dynamic planar graphs. In *2024 IEEE Topological Data Analysis and Visualization* (2024), IEEE, pp. 44–54. doi:10.1109/TopoInVis64104.2024.00009. 2, 3, 6, 7, 8, 10

[ROP11] ROPINSKI T., OELTZE S., PREIM B.: Survey of glyph-based visualization techniques for spatial multivariate medical data. *Computers & Graphics 35*, 2 (2011), 392–401. doi:10.1016/j.cag.2011.01.011. 3

[RPHL14] RISTOVSKI G., PREUSSER T., HAHN H. K., LINSEN L.: Uncertainty in medical visualization: Towards a taxonomy. *Computers & Graphics 39* (2014), 60–73. doi:10.1016/j.cag.2013.10.015. 3

[SBT*15] STEIGER M., BERNARD J., THUM S., MITTELSTÄDT S., HUTTER M., KEIM D. A., KOHLHAMMER J.: Explorative analysis of 2D color maps. In *WSCG 2015 Conference on Computer Graphics, Visualization and Computer Vision* (2015), Václav Skala – UNION Agency, pp. 151–160. URL: http://hdl.handle.net/11025/29437. 7

[Shn96] SHNEIDERMAN B.: The eyes have it: A task by data type taxonomy for information visualizations. In *Proceedings of IEEE Symposium on Visual Languages* (1996), IEEE, pp. 336–343. doi:10.1109/VL.1996.545307. 6

[SKR*24] STRAUB A., KARADIMITRIOU N., REINA G., FREY S., STEEB H., ERTL T.: Visual analysis of displacement processes in porous media using spatio-temporal flow graphs. *IEEE Transactions on Visualization and Computer Graphics 30*, 1 (2024), 759–769. doi:10.1109/TVCG.2023.3326931. 2

[SLSR08] SKEELS M., LEE B., SMITH G., ROBERTSON G.: Revealing uncertainty for information visualization. In *Proceedings of the working conference on advanced visual interfaces* (2008), ACM, pp. 376–379. doi:10.1145/1385569.1385637. 2, 4

[SMM12] SEDLMAIR M., MEYER M., MUNZNER T.: Design study methodology: Reflections from the trenches and the stacks. *IEEE Transactions on Visualization and Computer Graphics 18*, 12 (2012), 2431–2440. doi:10.1109/TVCG.2012.213. 8

[SNG*17] SCHULZ C., NOCAJ A., GOERTLER J., DEUSSEN O., BRANDES U., WEISKOPF D.: Probabilistic graph layout for uncertain network visualization. *IEEE Transactions on Visualization and Computer Graphics 23*, 1 (2017), 531–540. doi:10.1109/TVCG.2016.2598919. 2, 3

[SSSE16] SCHWANK J., SCHÖFFEL S., STÄRZ J., EBERT A.: Visualizing uncertainty of edge attributes in node-link diagrams. In *2016 20th International Conference Information Visualisation* (2016), IEEE, pp. 45–50. doi:10.1109/IV.2016.19. 3

[Sta14] STASKO J.: Value-driven evaluation of visualizations. In *Proceedings of the Fifth Workshop on Beyond Time and Errors: Novel Evaluation Methods for Visualization* (2014), ACM, pp. 46–53. doi:10.1145/2669557.2669579. 10

[VBW17a] VEHLOW C., BECK F., WEISKOPF D.: Visualizing group structures in graphs: A survey. *Computer Graphics Forum 36*, 6 (2017), 201–225. doi:10.1111/CGF.12872. 3, 6

[vBW17b] VON LANDESBERGER T., BREMM S., WUNDERLICH M.: Typology of uncertainty in static geolocated graphs for visualization. *IEEE Computer Graphics and Applications 37*, 5 (2017), 18–27. doi:10.1109/MCG.2017.3621220. 2, 3

[VHW25] VRIEND S., HÄGELE D., WEISKOPF D.: Two empirical studies on audiovisual semiotics of uncertainty. In *Proceedings of the 20th International Audio Mostly Conference* (2025), AM '25, ACM, pp. 107–123. doi:10.1145/3771594.3771604. 5

[vKS*11] VON LANDESBERGER T., KUIJPER A., SCHRECK T., KOHLHAMMER J., VAN WIJK J., FEKETE J.-D., FELLNER D.: Visual analysis of large graphs: State-of-the-art and future research challenges. *Computer Graphics Forum 30*, 6 (2011), 1719–1749. doi:10.1111/j.1467-8659.2011.01898.x. 2, 3

[WAM*19] WALL E., AGNIHOTRI M., MATZEN L., DIVIS K., HAASS M., ENDERT A., STASKO J.: A heuristic approach to value-driven evaluation of visualizations. *IEEE Transactions on Visualization and Computer Graphics 25*, 1 (2019), 491–500. doi:10.1109/TVCG.2018.2865146. 10

[Wei22] WEISKOPF D.: Uncertainty visualization: Concepts, methods, and applications in biological data visualization. *Frontiers in Bioinformatics 2* (2022), 793819. doi:10.3389/fbinf.2022.793819. 2

[YWL*22] YU D., WANG D., LUO Q., ZHENG Y., WANG G., CAI Z.: Stable structural clustering in uncertain graphs. *Information Sciences 586* (2022), 596–610. doi:10.1016/j.ins.2021.11.078. 3

[ZAH22] ZHANG D., ADAR E., HULLMAN J.: Visualizing uncertainty in probabilistic graphs with network hypothetical outcome plots (NetHOPs). *IEEE Transactions on Visualization and Computer Graphics 28*, 1 (2022), 443–453. doi:10.1109/TVCG.2021.3114679. 2, 3

[ZNL*17] ZHANG L., NGUYEN N. G. H., LAMBERT S., NICOT F., PRUNIER F., DJERAN-MAIGRE I.: The role of force chains in granular materials: from statics to dynamics. *European Journal of Environmental and Civil Engineering 21*, 7-8 (2017), 874–895. doi:10.1080/19648189.2016.1194332. 2